Journal of Materials Research and Technology 30 (2024) 9102–9114

Contents lists available at ScienceDirect

Journal of Materials Research and Technology

journal homepage: www.elsevier.com/locate/jmrt

Formation and influencing mechanism of the intermetallic compound in the friction stir welding of immiscible AZ31 and SPHC steel using aluminium powder as an additive

Sufian Raja [a,b,***], Farazila Yusof [a,b,c,*], Mohd Ridha Muhamad [a,b,**], Muhammad Safwan Mohd Mansor [a,b], Azib Juri [a,b], Bo Wu [a,b], Mohd Fadzil Jamaludin [b], Nooruddin Ansari [d], James Ren [e]

[a] Department of Mechanical Engineering, Faculty of Engineering, University of Malaya, 50603, Kuala Lumpur, Malaysia
[b] Centre of Advanced Manufacturing and Material Processing (AMMP Centre), University of Malaya, 50603, Kuala Lumpur, Malaysia
[c] Centre for Foundation Studies in Science (PASUM), University of Malaya, 50603, Kuala Lumpur, Malaysia
[d] Mechanical Engineering Program, Texas A & M University at Qatar, Qatar
[e] Faculty of Engineering and Technology, James Parsons Building, Liverpool John Moore's University, 3 Byrom St, Liverpool, L3 3AF, United Kingdom

ARTICLE INFO

Handling Editor:L Murr

Keywords:
Mg/Steel FSW
Microstructure analysis
Intermetallic compound
Welding and joining
Al powder additive

ABSTRACT

The primary issue with joining an immiscible magnesium/iron system is the lack of a bonding medium. This research used an aluminium (Al) additive as a bonding medium to facilitate the formation of an interface layer. Immiscible AZ31 magnesium alloy and SPHC low-carbon steel were successfully joined by employing aluminium (Al) powder as an additive in the gap between them with friction stir welding (FSW). The extensive interfacial microstructural analyses confirmed that the aluminium-rich Fe_2Al_5 intermetallic compound (IMC) formed with a range of 20–25 nm in thickness at the interface between magnesium and iron resulted from the metallurgical reaction between the Al powder additive and base SPHC steel. This IMC phase served as a transitional layer, facilitating the metallurgical bonding between Magnesium and Iron. The tensile strength of the joint was significantly improved by 43%, from 126 MPa without the additive to 180 MPa using the aluminium additive. The formation of the following well-matched interface lattice sites between Fe and Fe_2Al_5 region was identified: $(002)_{Fe2Al5}//(110)_{Fe}$, $[110]_{Fe2Al5}//[\bar{1}\ 13]_{Fe}$. The intermetallic Fe_2Al_5 was composed of nanocrystalline and amorphous interface layers. Furthermore, the fracture of the joint occurred at the interface, indicating a brittle mode of fracture behaviour.

1. Introduction

Research has been conducted on the possibility of using hybrid structures composed of different materials to reduce the vehicle's overall [1–4]. The use of a hybrid structure, achieved by welding and joining Mg alloys and steels, has been identified as an effective strategy for vehicle weight reduction while maintaining the required strength [5–7]. According to the Magnesium–Iron phase diagram, magnesium and iron are considered immiscible (unable to mix together) since the highest amount of Fe that can dissolve in Mg is merely 0.00043 wt% [8,9]. Hence, directly establishing a bond between Mg and steel is challenging [6,10,11].

A metallurgical interaction between the alloys of Mg and steel may be achieved through the diffusion of aluminium elements from the magnesium alloy workpiece and iron, forming the Fe_2Al_5 layer at the interface of welded joints [12–15]. Such a type of metallurgical bond was effectively achieved by the use of various welding methods, for instance, laser welding (LW) [16–18], cold metal transfer welding (CMT) [19–21], resistance spot welding (RSW) [22–24] and friction stir welding (FSW) [25–31]. These methods have a significant deal of promise for achieving a joint between steel and magnesium, which are incompatible with one another. Intermetallic layer formation is the

* Corresponding author. Department of Mechanical Engineering, Faculty of Engineering, University of Malaya, 50603, Kuala Lumpur, Malaysia.
** Corresponding author. Department of Mechanical Engineering, Faculty of Engineering, University of Malaya, 50603, Kuala Lumpur, Malaysia.
*** Corresponding author. Department of Mechanical Engineering, Faculty of Engineering, University of Malaya, 50603, Kuala Lumpur, Malaysia.
E-mail addresses: sufian@um.edu.my (S. Raja), farazila@um.edu.my (F. Yusof), ridha@um.edu.my (M.R. Muhamad).

https://doi.org/10.1016/j.jmrt.2024.05.249
Received 13 April 2024; Received in revised form 28 May 2024; Accepted 28 May 2024
Available online 29 May 2024

primary factor determining the integrity of the steel and magnesium joining, regardless of the technique used [12,32,33].

The FSW is a solid-state welding process that has demonstrated its effectiveness in joining materials that are both similar and different [34–40]. A significant amount of research has been conducted on the application of FSW for dissimilar materials joining. Based on these studies, one may get an understanding of the mechanism that allows different materials to join together [41–44]. Nevertheless, FSW has been employed to join low-carbon steel with AZ31 alloy [45,46]. An interface layer consisting of Fe_2Al_{13} was detected by joining Mg and steel without a trace of Zn. The use of zinc has improved the ability to weld AZ31 and steel together, resulting in an effective joining. It has been established by FSW of a variety of AZ-based magnesium alloys with steel that enhancing the amount of aluminium that exists in magnesium alloys results in an improvement in the mechanical characteristics of the joint. The experiment demonstrated that the AZ61 alloy, which contains a significant amount of aluminium, forms joints with the greatest strength, having Fe_2Al_5 IMC at the joint interface [47].

Due to the fact that the intermetallic layer plays a vital role in bonding magnesium and steel, many researchers have conducted extensive research on the interface layer. The CMT welding method was used to fabricate magnesium and steel dissimilar joints. A consistent and dense Al_2Fe intermetallic was produced at the joining interface of AZ61 and DP600 steel [48]. An investigation was conducted into the brazing capability of AZ31 alloy to tin-coated steel by employing the Mg–Al–Zn alloy-based filler material. It was found that the establishment of the joining of AZ31 with steel was facilitated by Fe–Al based IMC [49]. RSW was used to join the AZ31 with DP600 steel. The Fe_3Al nano IMC forms an effective bonding of AZ31 alloy with steel, resulting in a high-strength joining owing to the presence of low-energy interfaces [23].

Utilising the alloying elements from base workpiece materials is an easy and effective approach for joining magnesium and steel. Nevertheless, the formation of the IMC layer is affected by several factors, including the base material's chemical composition, the welding technique, and the inclusion of alloying elements from base workpiece materials. Consequently, it becomes challenging to control the development of the interface layer [50,51]. Moreover, it exacerbates the challenge of attaining robust welds, particularly for welding techniques such as FSW that operate at lower process temperatures, as the alloying element's diffusion from the base materials to the weld interface is limited [14,34,52].

Steel sheets and plates with low carbon have the advantages of excellent strength and a cost-effective manufacturing technique. It has found widespread application in many industries, such as machinery, shipbuilding, automotive, etc [53,54]. Steel pickle hot-rolled coil (SPHC) is a low-carbon steel that frequently finds applications for various automobile components, such as vehicle frames, wheels, and body bottoms [55,56]. Automotive parts fabricated from SPHC steel provide superior stiffness and strength, enhancing load-bearing capacity and strengthening energy absorption capability. Furthermore, SPHC steel is frequently employed to produce manufacturing components that seek convenient maintenance at inexpensive costs, such as vehicle frames [57]. Magnesium-based alloys frequently occur in several series, such as AM, AZ, ZK, ZE etc. Amidst these alternatives, AZ31 alloy is extensively used owing to its widespread availability in the marketplace and favourable mechanical properties [58,59].

Therefore, an aluminium powder additive was used in this study to achieve the goal of achieving improved joint properties in magnesium and steel welding. The AZ31 magnesium alloy and SPHC low carbon steel with Al powder at abutting faces were joined using FSW. The main aim of this research is to (a) realizing the bonding mechanism of AZ31 and SPHC steel and (b) establishing the orientation relationship between the nanoscale intermetallic interface layer and base materials.

Table 1
Chemical composition of base material.

Element	Mg	Al	Zn	Si	Mn	C	Fe
AZ31	Balance	2.80	0.60	0.10	0.15	–	–
SPHC Steel	–	–	–	0.01	0.27	0.05	Balance

2. Experimental

AZ31 magnesium alloy and low carbon steel, whose commercial name is steel pickle hot-rolled coil (SPHC) with JIS 3131 Japanese standard, were used as base material. Each workpiece had a dimension of 200 mm in length, 50 mm in width and 1.5 mm in thickness. The milled-certified chemical composition of the base material obtained from the supplier is depicted in Table 1. Aluminium powder (99.5% pure) with an average particle size of 5 μm was procured from Sigma-Aldrich.

Manford VL-610 vertical CNC milling machine equipped with an FSW fixture was used for experimentation. The pneumatic clamp was used to clamp the workpiece. The advantage of the pneumatic clamp over conventional nut and bolt arrangement is uniform pressure distribution and ease of clamp-unclamp of workpieces.

FSW was performed using a welding tool made from tungsten carbide with a shoulder diameter of 12 mm, 1.3 mm length of tool pin and 4 mm pin diameter, as shown in Fig. 1 (a). The workpiece was placed in a butt configuration in which SPHC steel was kept at the advancing side, and AZ31 was kept at the retreating side. The faying surface of the workpieces was cleaned with acetone to remove contamination and dirt. Tool offset was taken as 0.5 mm into the steel. Prior to welding, a gap of 0.5 mm was filled with the Al powder additive, as shown in Fig. 1 (b). Welding was performed with the tool rotation speed of 500 rpm and welding speed of 50 mm/min, as depicted in Fig. 1 (c). In addition, the FSW of AZ31 and SPHC steel was performed for comparison purposes without any additives using similar process parameters.

A wire electrical discharge machine cut samples for tensile test and metallographic analysis. Specimens for tensile testing were prepared according to ASTM: E8 sub-size standard, as shown in Fig. 1 (d). Tensile test was performed using the universal testing machine (Instron-3369) with a 0.5 mm/min pull rate. The sample for microstructure was taken from the cross-section of the welded specimen and successively grounded and polished with 0.5 μm alumina suspension. Microstructural characterization was performed using optical microscopy and scanning electron microscopy equipped with energy-dispersive spectroscopy (SEM-EDS). The macroscopic view of samples was observed with Olympus (Origin- Tokyo, Japan) optical microscope. The microscopic characteristics were observed with SEM-EDS equipment (Model: Hitachi, SU8030) with an accelerating voltage of 5 kV–15 kV in order to get images and EDS analysis.

TEM lamella was prepared using the FEI Helios dual beam instrument. Fig. 2 shows steps to prepare thin lamella with a thickness of less than 100 nm for TEM-EDS analysis. Fig. 2 (a) shows the AZ31 and SPHC steel interface from where the TEM lamella sample was extracted. Fig. 2 (b)–(d) shows the slicing of the lamella until the thickness is less than 100 nm. The lamella was picking up and mounting on the Cu-grid, as shown in Fig. 2 (e)–(f). TEM-EDS analysis was performed using FEI Tecnai G2 F20 TEM. The TEM machine was equipped with EDS. TEM imaging was performed at 300 kV accelerating voltage. EDS analysis was performed at different locations to know about elemental composition at the nanoscale level.

3. Result and discussion

3.1. Welded joint surface appearance

Welded joints exhibited excellent surface appearances without any flash formation. Fig. 3 shows the surface appearance of the FSW joint

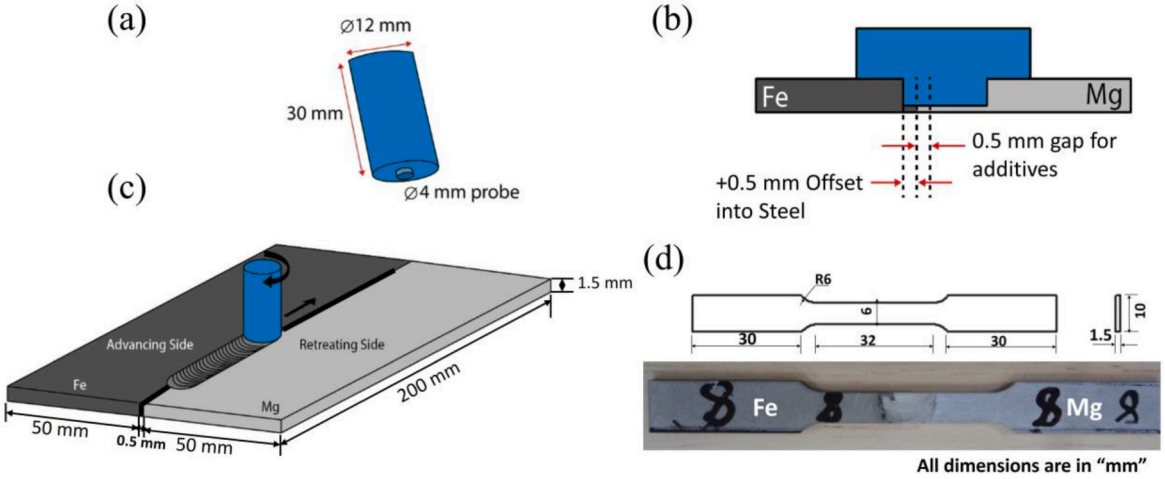

Fig. 1. Schematic of FSW process (a) FSW tool, (b)schematic diagram of tool-offset and gap for additive (c) FSW process, (d) Standard tensile tests specimen.

with and without the addition of the Al additive.

The addition of Al powder resulted in an improved surface finish of the joint, as seen by comparing Fig. 3(a) and (b). Fig. 3 (a) shows the surface of the welded joint without any additive. A boundary between AZ31 and SPHC can be clearly seen. However, this distinct boundary disappeared in the welded sample with the Al additive, as shown in Fig. 3 (b), which is believed to be due to the uniform mixing of the Al additive during welding. Lastly, none of the joints had defects like tunnels, voids or pores.

3.2. Macrostructural observation of cross-section

The cross-sectional microstructure of typical FSWed AZ31 and SPHC steel without additive and with Al powder additive is depicted in Figs. 4 and 5, respectively.

Fig. 4 depicts the steel strip inserted into the magnesium side. The insertion of a large steel strip into the magnesium side is mostly associated with the plastic flow behaviour of the materials. The base AZ31 magnesium alloy exhibits an equiaxed grain structure, whereas SPHC steel has a grain structure consisting of ferrite grains owing to its low carbon content, as shown in Fig. 4 (a) and 4 (d). Fig. 4 (b) and 4 (c) depict the microstructure of the stir zone for AZ31 magnesium alloy and SPHC steel. It is evident that the tool's stirring actions cause significant deformation in the grains of both AZ31 magnesium alloy and SPHC steel near the interface.

In Fig. 5, the materials were mixed in an alternating manner to create an intricate layered structure. The results showed that the shorter steel strips established a beneficial mechanical interlocking, which effectively enhanced the strength of the joints. Fig. 5 (a) shows the AZ31 magnesium alloy with grains that are equiaxed in shape. Furthermore, inside the area where stirring occurs, equiaxed grains are formed with a smaller grain size, as seen in Fig. 5 (b). The grains of AZ31 in the stir zone underwent recrystallization and were transformed into smaller, equiaxed grains. Due to the adverse heat input circumstance, the development of magnesium grain did not occur after the tool probe had passed through the system. Similarly, the area where stirring occurs on the mild steel side shows finer grains than the base SPHC steel, as depicted in Fig. 5 (a) and 5 (b), respectively.

In FSW, the stir zone experiences the most extreme thermal cycle and endures substantial plastic deformation. This leads to the occurrence of dynamic recrystallization (DRX) and the refinement of grain structure. Since the material surrounding the stir zone is subjected to plastic deformation as a consequence of the shear stress that is delivered by the tool, the thermomechanically affected zone (TMAZ) is formed as a result. The TMAZ is mainly composed of smaller grains that are equiaxed in shapes and grains that have been partially modified. The normal grain size of the TMAZ is considerably larger than that of the stir zone [60].

3.3. Interfacial characterisation and tensile properties analysis

Fig. 6 (a) shows the cross-sectional SEM image for AZ31 and SPHC steel FSW without any additive. Fig. 6 (c) depicts the high-magnification micrograph of the highlighted interface region highlighted in Fig. 6 (a) without any apparent interface layer. Fig. 6 (d)–(f) shows the line EDS line scanning across the interface. A region with an elevated concentration of aluminium is seen at the interface between magnesium and steel, as shown in Fig. 6 (e). The interface line scanning findings indicate that the interface layer mostly consists of iron and aluminium. However, the intensity count of aluminium is relatively low, which could be a reason for the non-existence of an apparent interface layer. The concentration of aluminium at the interface of the AZ31/SPHC steel is very low, making it challenging to detect any variations in the Al content.

Fig. 6 (b) shows the cross-sectional SEM image for AZ31 and SPHC steel FSW with Al additive. The SEM image with high magnification depicted in Fig. 6 (g) is taken from the area encircled in Fig. 6 (b). It can be seen that an interface layer appeared in FSWed AZ31/SPHC steel with Al additive. Subsequently, Fig. 6 (h)–(j) shows the EDS line scanning across the interface for welded sample with Al additive. The intensity of the Al-enriched region exhibits significant variation, as seen by the line scanning depicted in Fig. 6 (i). This significantly increased and fluctuated aluminium concentration due to the Al additive, which could help in the formation of the IMC. Due to apparent visibility of the IMC in AZ31/SPHC welding with Al additive, further analysis will be followed with this welding condition to realize the influence of Al additive in interface layer formation with improved joint properties.

In order to gain a more explicit understanding of the joint's interfacial structure, a specific interface region was enlarged, and the resulting morphology is shown in Fig. 7. The EDS elemental spectra provide the elemental composition for points 1–3. Based on the information shown in Fig. 7, it is evident that an increase in the concentration of aluminium Al element is seen at the interface between AZ31 and steel. When the tool is stirred along the joint line, the exertion of heat and force causes the diffusion of the aluminium additive into the base steel. As a result, there is an increase in the concentration of Al elements at the interfacial region. The EDS examination of point 2 in Fig. 7 indicates that it predominantly comprises an Al-rich intermetallic layer (70.6% Al and 29.3% Fe).

A SEM-EDS mapping analysis was performed to determine the distribution of aluminium additives. Fig. 8 demonstrates the uniform distribution of aluminium along the interface between magnesium and

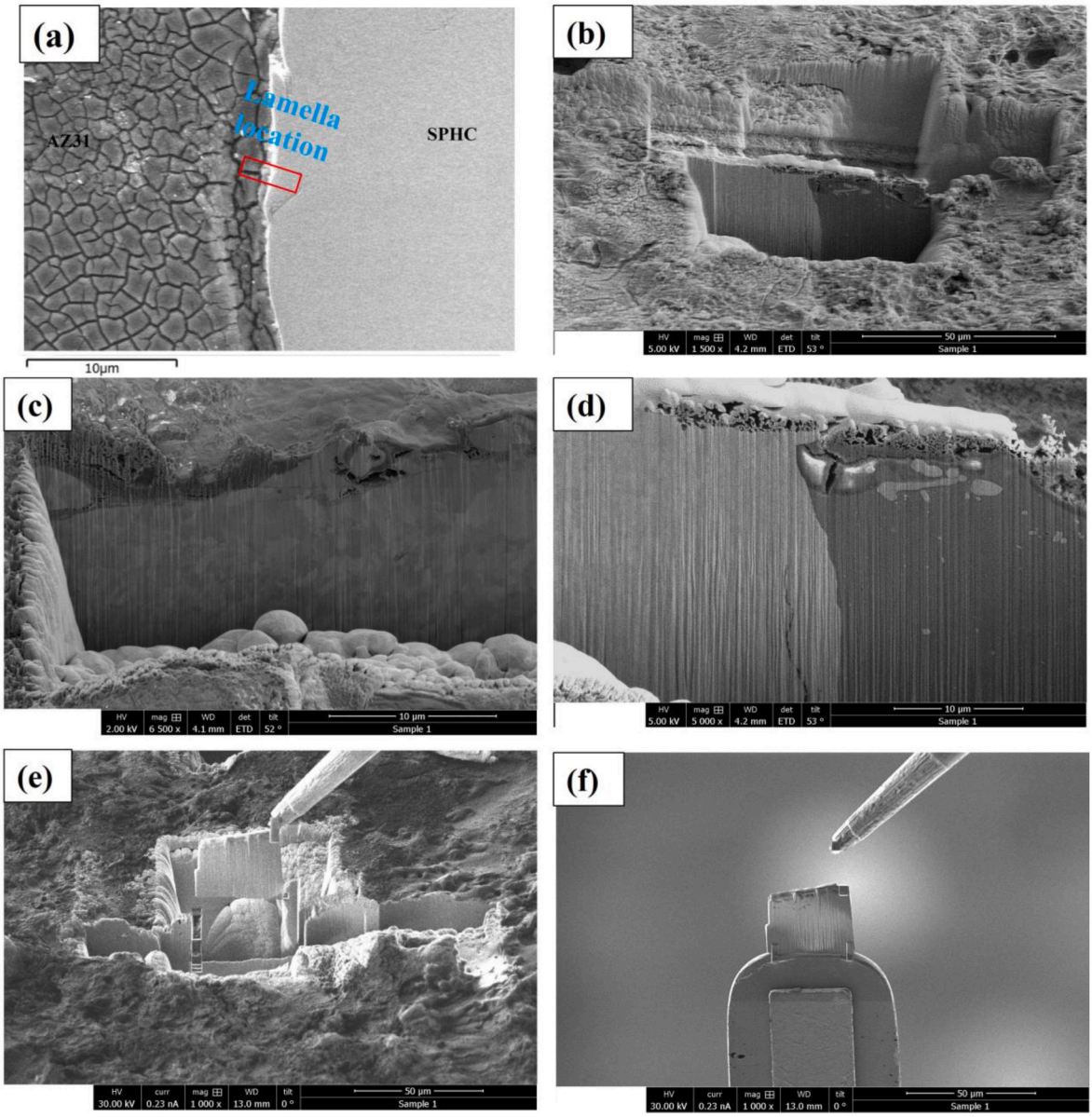

Fig. 2. Lamella preparation using dual-beam from the interface of AZ31/SPHC (a) AZ31/SPHC interface (b–d) digging of trench all around lamella (e) picking up of lamella (f) lamella mounted on a copper grid.

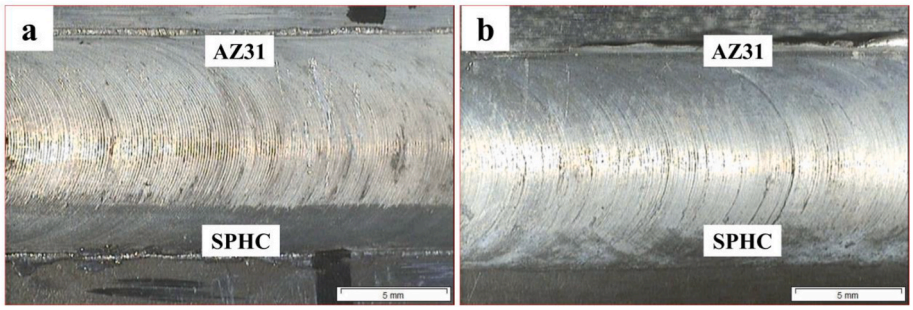

Fig. 3. Surface Appearance of AZ31 and SPHC steel (a) without additive, (b) with Al powder additive.

steel, which verifies the high-intensity aluminium concentration of line scanning in Fig. 6 (i) and spot analysis in Fig. 7. An effective bond between immiscible materials occurs when an IMC forms along the joint line. The alloying elements present in the base materials are consumed to form the intermetallic compound during the welding process of immiscible materials, namely between magnesium alloy and steel [51]. To control the reduction of the alloying components from the base workpiece materials, one may use second-phase particles as additives to

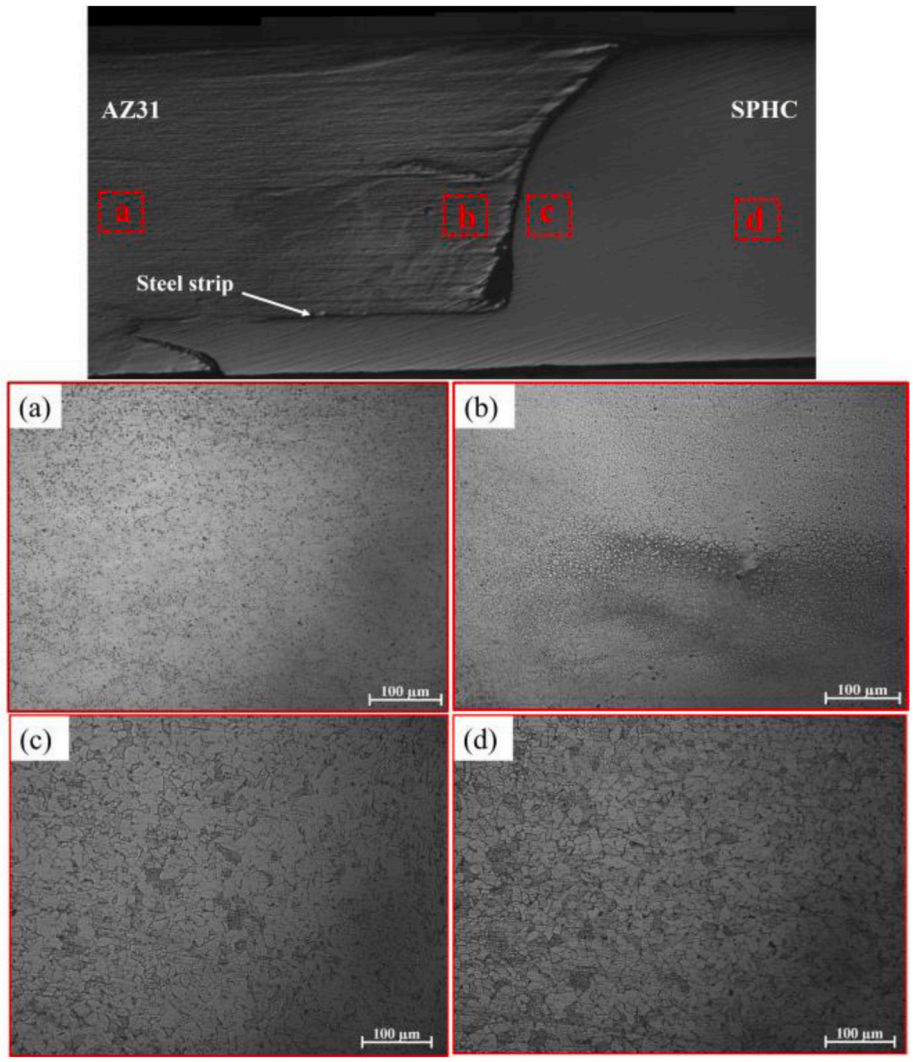

Fig. 4. Cross-sectional macrograph of AZ31 and SPHC steel without additive (a) base AZ31 magnesium alloy, (b) AZ31 side of stir zone, (c) SPHC steel side of stir zone, (d) base SPHC steel.

maintain the elemental content of the base workpiece.

Using aluminium additions led to higher tensile strengths compared to specimens without powder additives. The specimen containing Al powder additions attained a tensile strength of 180 MPa, as seen in Fig. 9 (a). The tensile strength of the specimen with powder additions is 43% higher than the specimen without additives. The reduced strength of the welded specimen without the additive may be attributed to the immiscibility of magnesium and iron, resulting in the absence of an interface layer, leading to poor joint formation. Based on the observation of the stress-strain curve from Fig. 9(b), it is evident that the elongation is low in the absence of additives. This is likely because no visible interfacial layer is present at the AZ31/SPHC steel interface, which is responsible for reducing the strength and elongation.

3.4. Role of Al additive in the formation of IMC in the FSW process

The welded interface between AZ31 and SPHC steel with Al additive has been analysed using high-magnification SEM images, shown in Figs. 6–8. These images reveal the presence of a visible interfacial layer. The EDS line scan from AZ31 to SPHC steel workpiece reveals a gradual variation in the intensity of aluminium at the interface, as seen in Fig. 6 (i). The EDS spot analysis in Fig. 7 shows that the interface consists of 70.6 at. % of Al and 29.3 at. % of Fe. EDS elemental mapping has shown an enrichment of aluminium along the interface, as seen in Fig. 8. The findings from elemental line EDS, spot EDS, and elemental mapping indicate the formation of an aluminium-rich IMC near the joint interface.

The development of IMC is a process that is regulated by diffusion and occurs in three distinct stages. The first stage encompasses the diffusion of iron and aluminium atoms, but their solubility is limited [61]. Furthermore, it is worth noting that the aluminium and iron diffusion coefficients are very low. Specifically, the iron's diffusion coefficient into Aluminium is 53×10^{-4} m^2/s (at temperatures ranging from 793 to 922 K), while the aluminium's diffusion coefficient into Iron is 1.8×10^{-4} m^2/s (at temperatures ranging from 713 to 733 K) [62,63]. The solid solution undergoes a process where it produces an intermetallic compound in the second step after its elemental composition approaches the saturation point. This is subsequently followed by the growing of the intermetallic compound thicknesses in the third step. The thickness of the intermetallic compound is determined by the reaction time (t) at a specific temperature and pressure, which can be calculated using the fundamental kinematics equations (1) and (2) [61].

$$S = Kt^x \tag{1}$$

$$K = K_0 \, exp\left(\frac{-Q}{RT}\right) \tag{2}$$

The variables in the equation are defined as follows: K represents the

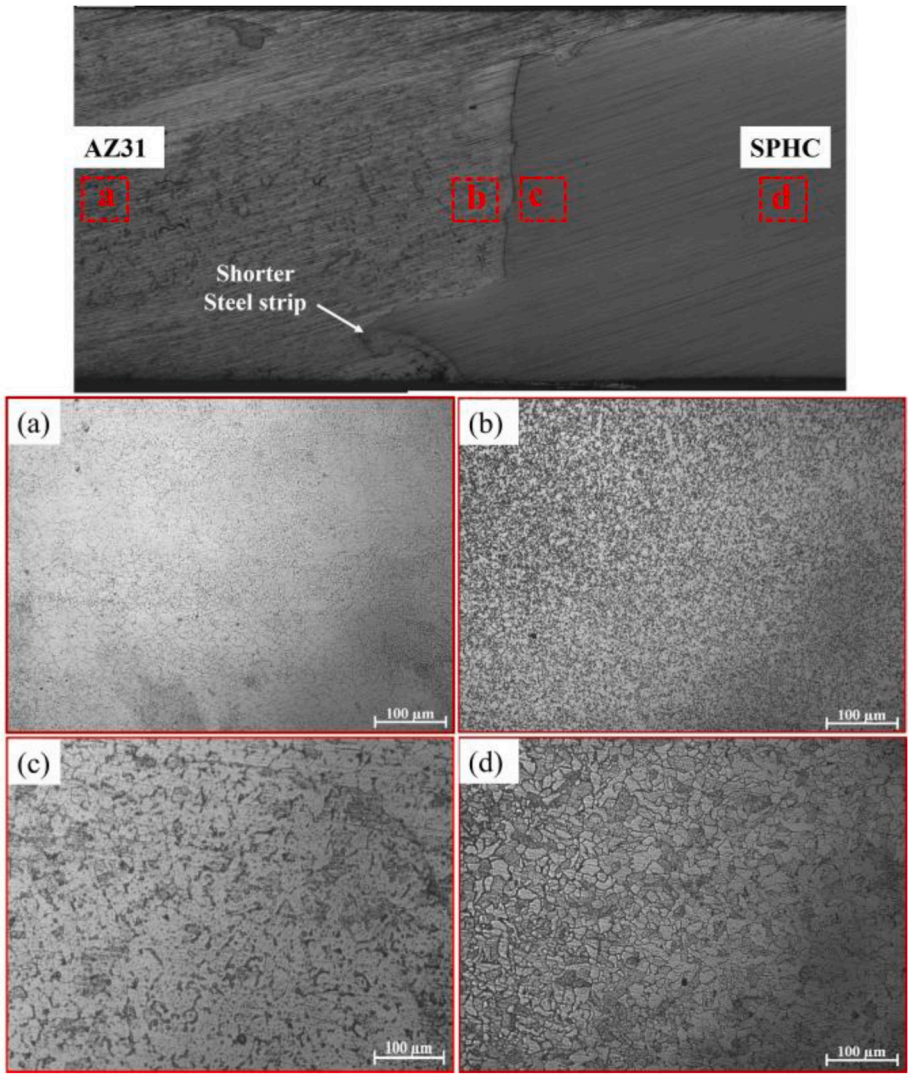

Fig. 5. Cross-sectional macrograph of AZ31 and SPHC steel with Al additive (a) base AZ31 magnesium alloy, (b) AZ31 side of stir zone, (c) SPHC steel side of stir zone, (d) base SPHC steel.

"rate constant", K_0 represents the "pre-exponential factor", Q represents the "chemical activation energy" in joules per mole, x represents the "exponential factor", R represents the "universal gas constant" in Joules per Kelvin per mole, and T represents the "reaction temperature" in kelvin. While the activation energy for aluminium and iron for Fe_2Al_5 may vary from 74 kJ mol^{-1} to 281 kJ mol^{-1}, it is essential to note that this energy varies following the temperature of the reaction [64]. The development of intermetallic compounds between aluminium and iron typically occurs at temperatures over 600 °C and under atmospheric pressure. However, in the case of the FSW, IMC may form at the weld interface even at temperatures below 600 °C. This is attributed to the intense plastic deformation and pressure applied by the friction stir welding tool.

Fig. 10 depicts an illustration that explains the changes in the microstructure of the joint interface between AZ31 and SPHC steel with Al additive. Before FSW, the AZ31 workpiece is placed on the retreating side, while the steel workpiece is on the advancing side. The heat generated from the rotation of the welding tool is transferred to the interface by the process of thermal conduction. Fig. 10 (a) illustrates the starting condition of the welding process. During the welding process, the application of heat and pressure causes the diffusion of aluminium additives towards the interface, creating a new layer at the interface, as depicted in Fig. 10 (b). When the heat input during welding is reduced, as is the case with FSW, the aluminium elements at the joint interface react with iron elements, forming aluminium-rich Fe–Al intermetallic compounds. Fig. 10 (c) and (d) depict the interfacial layer's arrangement.

3.5. Bonding orientation relationship (OR) of AZ31 and SPHC steel interface layer

The line scan analysis using SEM-EDS of the AZ31 and SPHC steel with Al additive, as shown in Fig. 6 (i), indicated significant fluctuations in the aluminium elements in the near interface area. Further analysis through spot analysis and elemental mapping, depicted in Figs. 7 and 8, divulged that the joint interface primarily comprises Fe–Al IMC with a high concentration of aluminium. However, the SEM-EDS analysis could not accurately and reliably determine the composition of the interface layer. Therefore, TEM and TEM-EDS spot analysis was used to conduct a more in-depth analysis of the interface.

A continuous and uniform nanolayer of IMC ranging from 20 to 25 nm in thickness was clearly detected at the interface, as shown in Fig. 11 (b). The SAED of IMC is depicted in the inset of Fig. 11 (b). The presence of a nanolayer IMC between the aluminium and iron elements was verified using TEM-EDS spot analysis in Fig. 11 (c). At interface point 3 in TES-EDS, the counts of aluminium and iron were high, suggesting the

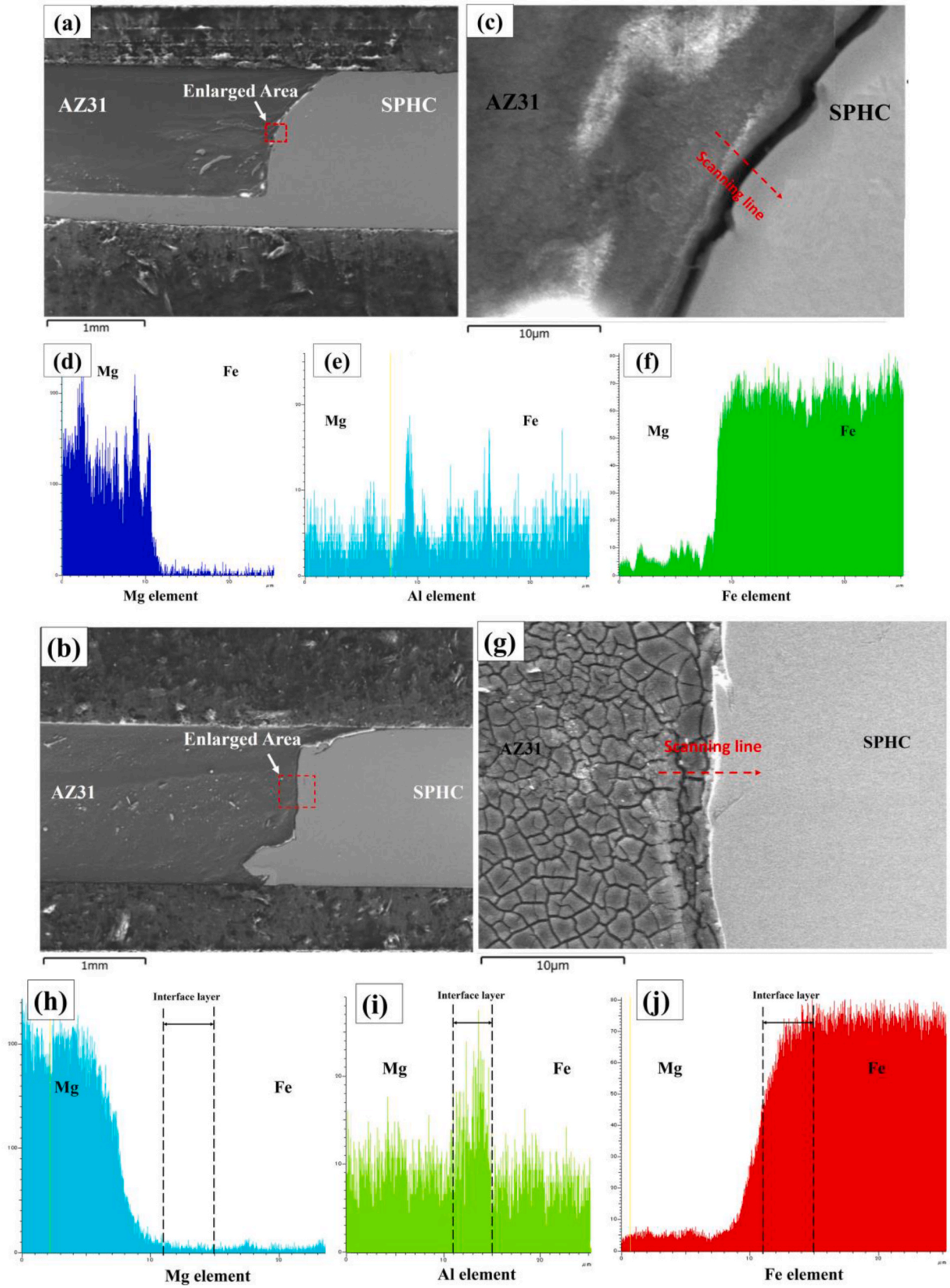

Fig. 6. (a)–(b) Cross-section of AZ31/SPHC steel and AZ31/SPHC steel with Al additive (c)–(f) AZ31/SPHC steel without additive interface morphology with EDS line scanning, (g)–(j) AZ31/SPHC steel with Al additive interface morphology with EDS line scanning.

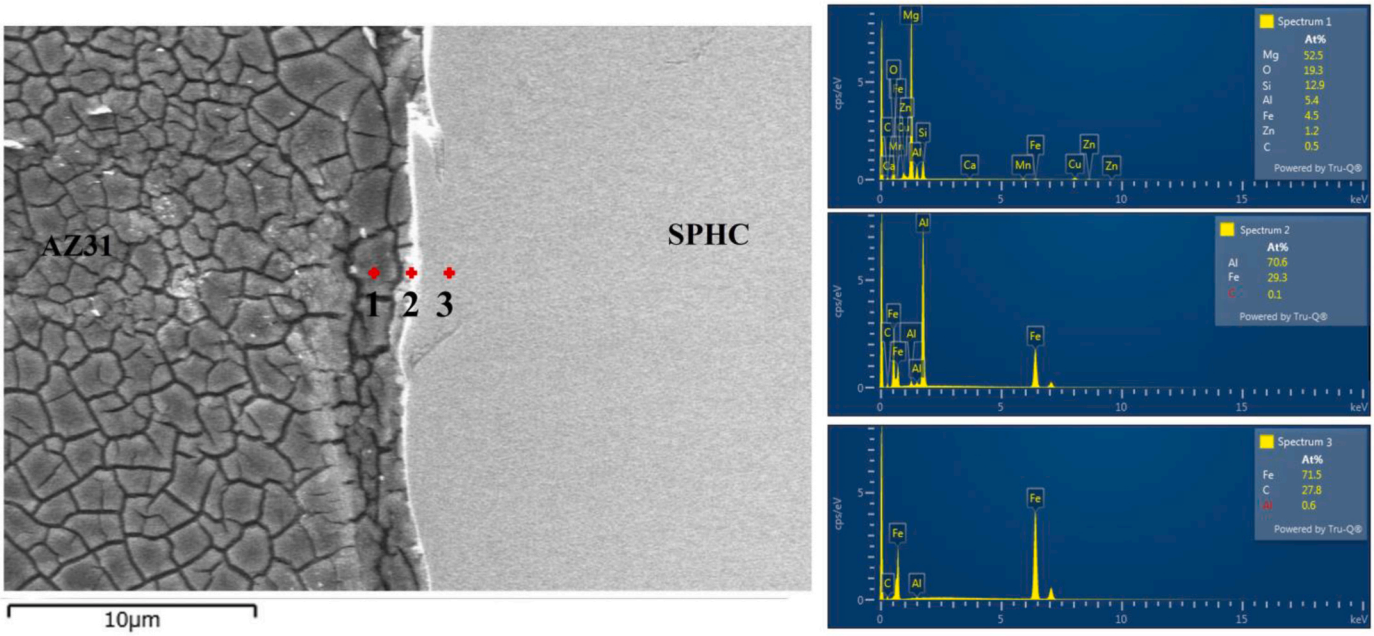

Fig. 7. Interface morphology AZ31/SPHC steel using Al additive with EDS spot spectra.

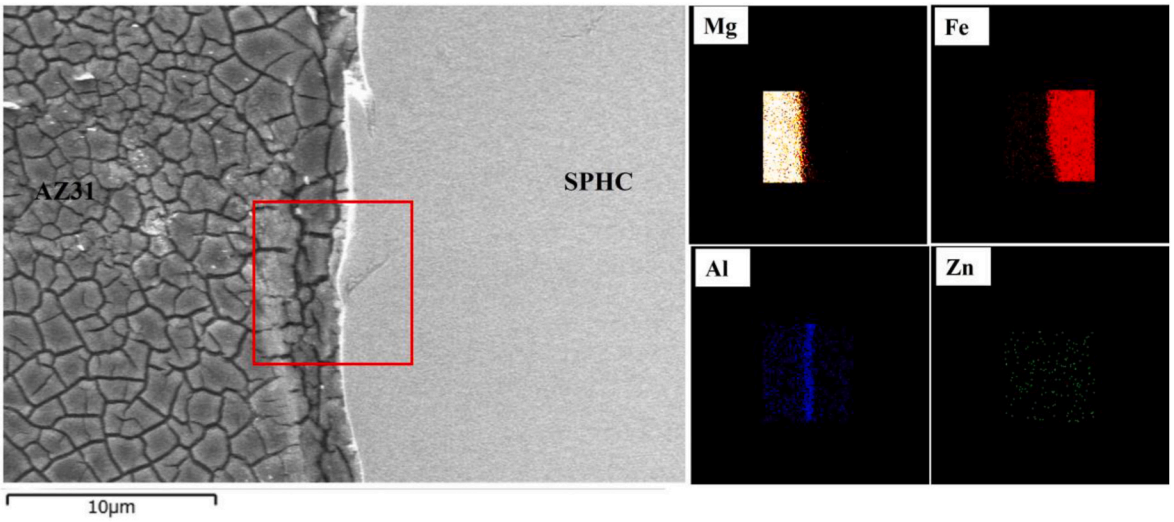

Fig. 8. EDS mapping of AZ31/SPHC steel interface with Al additive.

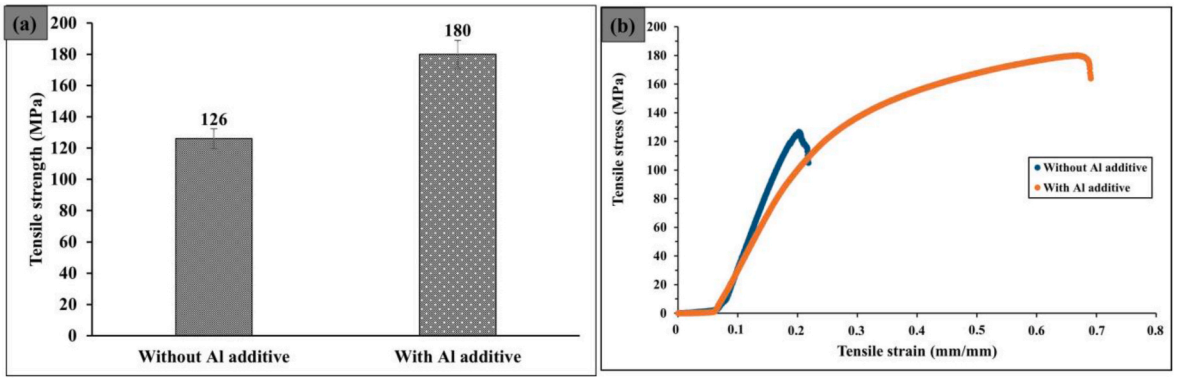

Fig. 9. (a) Tensile strength of joint with and without additive, (b) stress-strain curve.

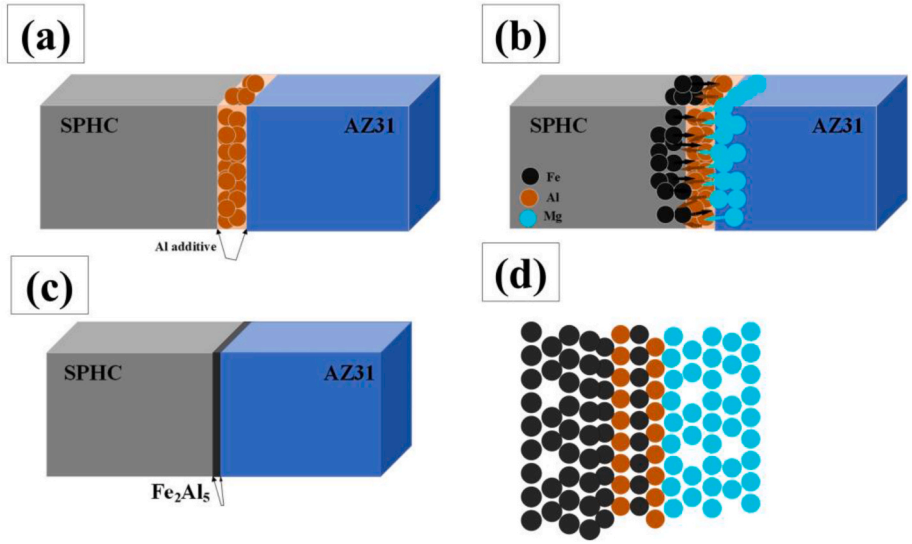

Fig. 10. Schematic diagram of AZ31 and SPHC FSW joint using Al additive (a) Initial welding state (b) Formation IMC during FSW (c) Formation of joint with interfacial layer (d) schematic of Fe–Al IMC.

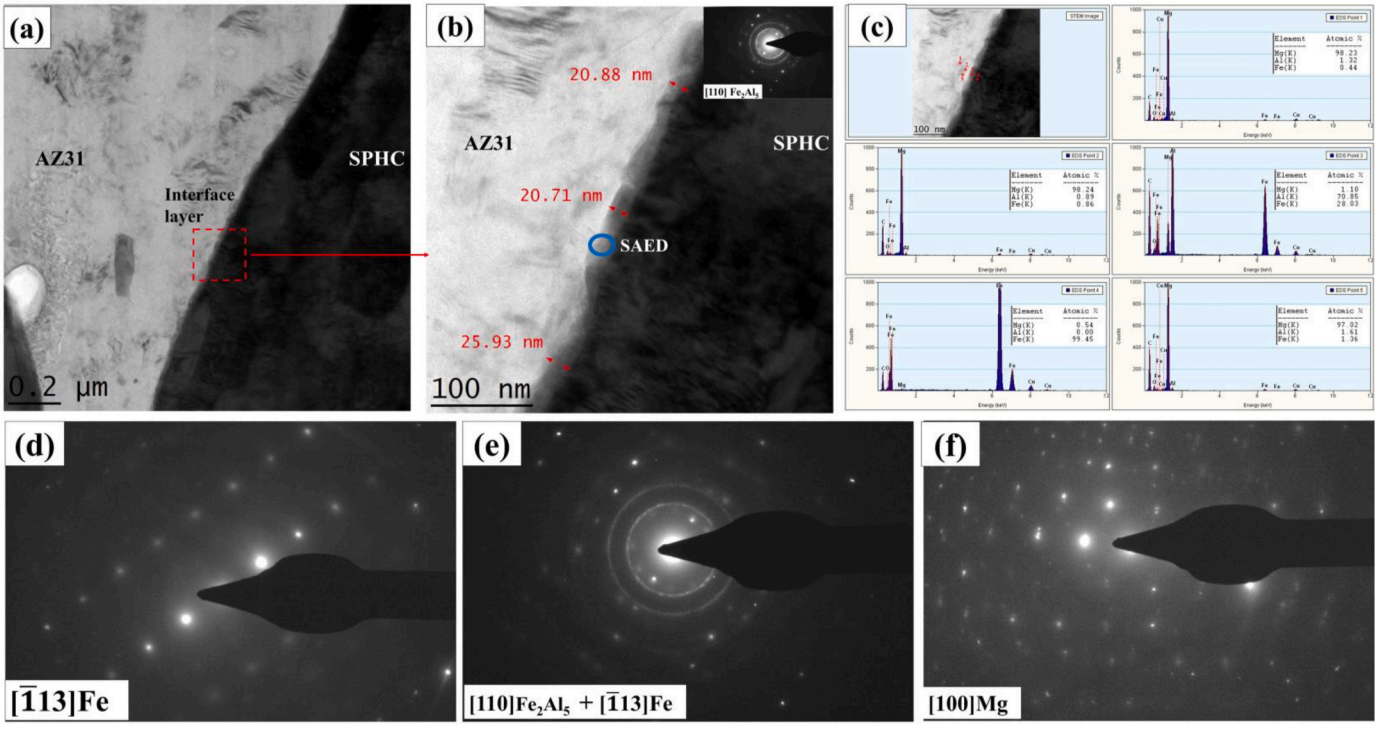

Fig. 11. TEM analysis of interface (a) TEM image of AZ31/SPHC steel interface (b) TEM image showing IMC thickness and corresponding SAED of IMC in inset (c) TEM-EDS spot analysis across the interface (d–e) diffraction pattern, parallel to $[110]_{Fe2Al5}$ and $[\bar{1}\ 13]_{Fe}$, (f) diffraction pattern of Fe_2Al_5/Mg interface.

presence of IMC composed of Al and Fe. The study revealed that the IMC consisted of 70.85 at.% Al and 28.03 at.% Fe, which confirms the Fe_2Al_5 intermetallic compound formation.

The bonding OR of the Fe/Fe_2Al_5 interface and Mg/Fe_2Al_5 interface were obtained using SAED [Fig. 11 (e)–(f)]. SAED image, as shown in Fig. 11 (e), was obtained in a consistent orientation without any inclination, following the zone axis of $[110]_{Fe2Al5}$ and $[\bar{1}\ 13]_{Fe}$. The diffraction pattern of the $(002)_{Fe2Al5}$ was superimposed with the diffraction pattern of the $(110)_{Fe}$, as illustrated in Fig. 11 (e). This revealed that the OR of the Fe and Fe_2Al_5 was: $(002)_{Fe2Al5}//(110)_{Fe}$, $[\bar{1}\ 13]_{Fe}//[110]_{Fe2Al5}$. It was observed that the Fe–Al intermetallic compound may develop on ferrite grains. This results in the formation of Fe_2Al_5, which exhibits clear orientation relationships with the Fe workpiece, such as $(1\ \bar{1}\ 0)_{Fe2Al5}//(2\ \overline{11})_{Fe}$, $(001)_{Fe2Al5}//(0\ \bar{1}\ 1)_{Fe}$ and $[110]_{Fe2Al5}//[111]_{Fe}$ [65]. As depicted in Fig. 11 (e), an orientation relationship of $(002)_{Fe2Al5}//(110)_{Fe}$, $[\bar{1}\ 13]_{Fe}//[110]_{Fe2Al5}$ was discovered for the Fe and Fe_2Al_5 interface in this work. It is implied that this orientation relationship leads to a low-energy interface [66]. As a result, steel and Fe_2Al_5 IMC have the potential to form a strong bond.

An absence of a superimposed diffraction spot at the Fe_2Al_5/Mg interface was noticed. However, the theoretical calculation of the orientation relationship between Fe_2Al_5 and Mg is possible. According to

Table 2
Potential planes and orientations that may be matched between Fe_2Al_5 and Mg in FSW.

Matching Planes or directions	$(0002)_{Mg}$// $(021)_{Fe2Al5}$	$(022)_{Fe2Al5}$// $(01\text{-}1\text{-}2)_{Mg}$	$[4\text{-}2\text{-}20]_{Mg}$// $[0\text{–}10]_{Fe2Al5}$	$[4\text{-}2\text{-}20]_{Mg}$//$[1\text{-}12]_{Fe2Al5}$
d-Spacing (nm) **Mg**	0.261	0.190	0.642	0.642
d-Spacing (nm) **Fe_2Al_5**	0.255	0.211	0.642	0.654
Mismatch (%)	2.3	10.5	0	1.9

the orthorhombic Fe_2Al_5 lattice parameters, $a = 0.7649\,nm$, $b = 0.6413\,nm$, and $c = 0.4217\,nm$; and HCP Mg lattice parameters, $a = 0.3209\,nm$ and $c = 0.5211\,nm$, potential planes and orientations that may be matched between Fe_2Al_5 and Mg are presented in Table 2. To get the interatomic and interplanar misfits for Fe_2Al_5 and Mg interface, the following formula (3) is utilised:

$$\delta = \frac{|\Delta a_0|}{(a_0)} \tag{3}$$

Δa_0 = Difference between interplanar or interatomic distance
a_0 = respective Fe_2Al_5 interplanar or interatomic distance

Table 2 indicates that the $[0\text{–}10]_{Fe2Al5}$//$[4\text{-}2\text{-}20]_{Mg}$ and $[1\text{-}12]_{Fe2Al5}$//$[4\text{-}2\text{-}20]_{Mg}$ direction mismatch is slight, which is found to be 0% and 1.9%, respectively. Additionally, the interplanar mismatching of $(021)_{Fe2Al5}$//$(0002)_{Mg}$ and $(022)_{Fe2Al5}$//$(01\text{-}1\text{-}2)_{Mg}$, is also minimal and found to be 2.3% and 10.5%, respectively. These results based upon the orientation relationships suggest that the lattice locations of Fe, Al5Fe2, and Mg are in agreement, indicating that Al5Fe2 might be used as a possible intermetallic compound layer to achieve improved strength in friction stir welding of magnesium alloys to steels.

Diffraction rings were seen in the SAED pattern of the intermetallic compound region shown in Fig. 11 (b). This suggests that the IMC layer may consist of a combination of crystalline and amorphous compounds. Hence, conducting the HRTEM investigation of the IMC layer is essential.

Fig. 12 displays the HRTEM analysis of the interface between magnesium and steel. Fig. 12 (a) displays the HRTEM image illustrating the

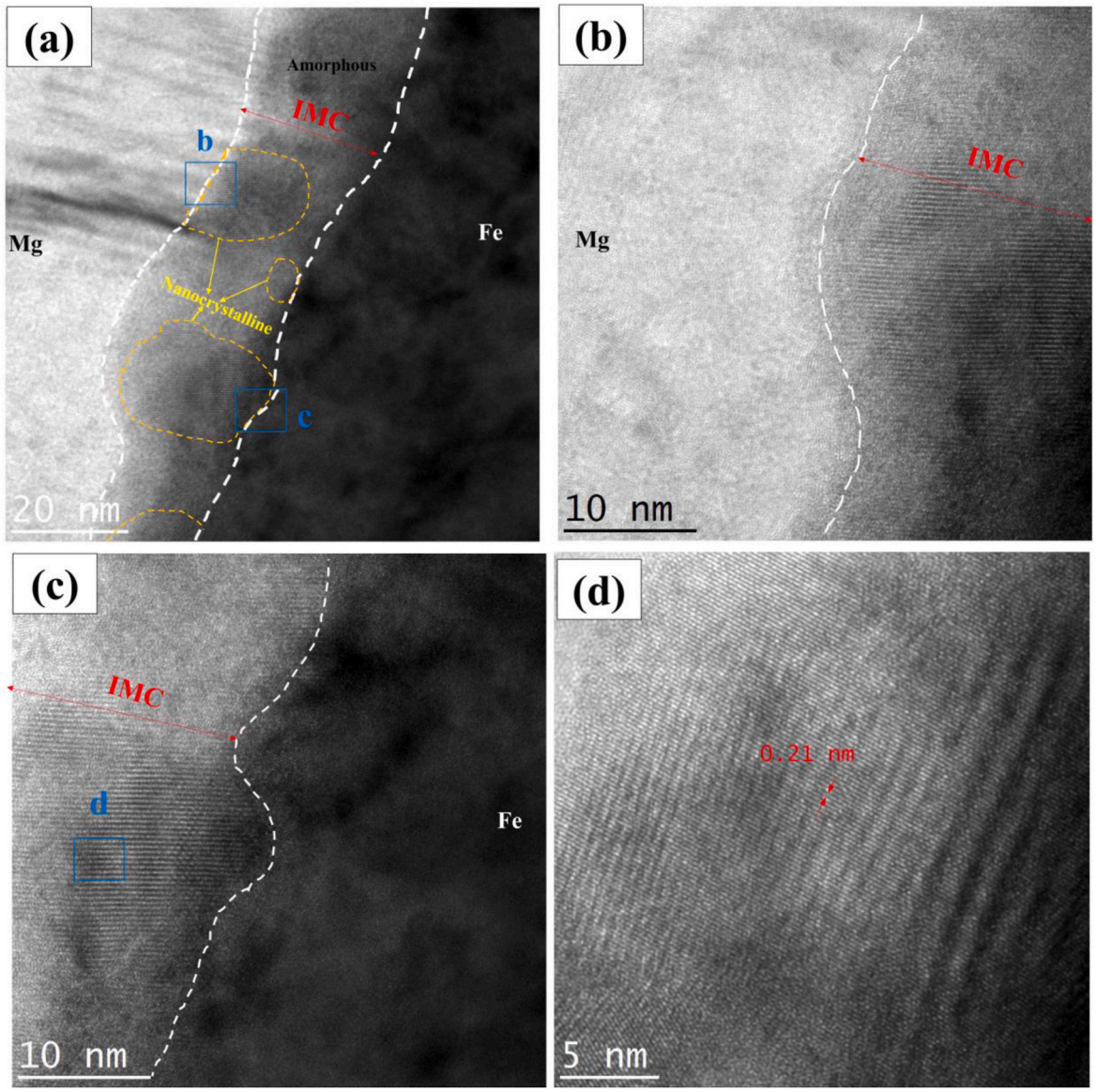

Fig. 12. HRTEM analysis (a) Mg/IMC/Fe image (b) HRTEM image Mg/IMC (c) HRTEM image of IMC/Fe (d) HRTEM image of Fe_2Al_5.

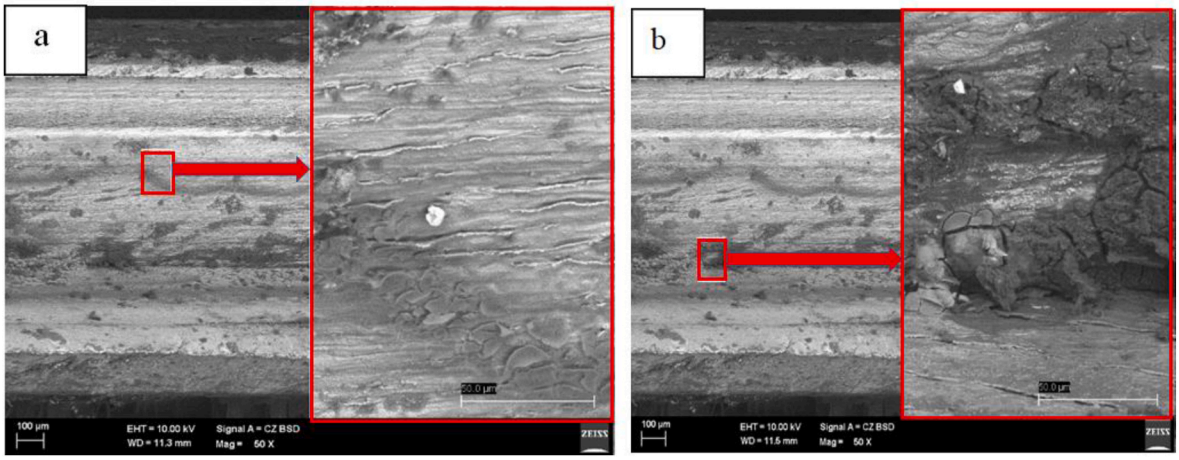

Fig. 13. SEM of fractured surface: (a) featureless region and (b) cracking of an agglomerated aluminium.

IMC layer between Mg and steel. There are no consistent patterns present in the IMC layer. The IMC layer exhibits intermittent lattice fringes, mainly consisting of nanocrystalline structures, whereas the majority of the area in the IMC layer remains amorphous. Fig. 12 (b) shows the HRTEM image of Mg/Fe_2Al_5, depicting the amorphousness and nanocrystallinity of the IMC. The region of the Fe_2Al_5, located nearer to the Mg side, consists of the amorphous structure. Fig. 12 (c) displays the HRTEM image of Fe_2Al_5/steel, revealing the amorphousness and nanocrystallinity of the IMC, as in the previous case. However, the region of the Fe_2Al_5, located nearer to the steel interface, consists of the nanocrystalline structure, with a few distant areas exhibiting amorphousness. Fig. 12 (d) shows lattice fringes of the Fe_2Al_5 IMC's nanocrystalline region, which were found to be 0.21 nm.

3.6. *Fractography of specimen with Al additive*

Fig. 13 depicts the SEM images of the fractured tensile workpiece with Al powder additive. Fig. 13(a) depicts the area of the fractured surface where the lack of the Al additive was seen in a localised manner. Fig. 13(b) exhibits a satisfactory distribution of Al particles after FSW, allowing increased surface exposure for intense deformation caused by the effects of friction and temperature exposures. In addition, the interface additionally displays Al powder additive agglomerates in specific locations. Based on the fractography analysis, it was determined that the FSWed sample experienced fracture at the joint interface.

4. Conclusions

Friction stir welding of immiscible AZ31 magnesium alloy and SPHC steel using Al powder as an additive was successfully achieved, and the formation and influencing mechanism of the intermetallic compound was investigated. The following conclusions are drawn.

1. The specimen containing Al powder additions attained an improved tensile strength of 180 MP compared to 126 MPa without the additive. The tensile strength of the specimen with powder additions is 43% higher than that of the specimen without additives.
2. A continuous and uniform nanolayer of Al-rich Fe_2Al_5 intermetallic compound with a thickness ranging from 20 to 25 nm was formed at the interface. The IMC layer consists of the amorphous structure as well as nanocrystalline structures featuring lattice fringes. In other words, IMC consists of an amorphous-nanocrystalline structure.
3. Low energy and well-matched lattice sites were observed between Fe and Fe_2Al_5 Interface. Orientation relationship of $(002)_{Fe2Al5}$// $(110)_{Fe}$, $[\bar{1}\ 13]_{Fe}$//$[110]_{Fe2Al5}$ was identified for the Fe and Fe_2Al_5 interface.

Declaration of competing interest

The authors declare that they have no known competing financial interests or personal relationships that could have appeared to influence the work reported in this paper.

Acknowledgement

The authors would like to acknowledge the University of Malaya, Malaysia, for providing the necessary facilities and resources for this research. This research is supported by the Fundamental Research Grant Scheme (FP087-2023) funded by the Ministry of Higher Education, Malaysia and the EU H2020 project, MSCA-RISE-2018 (i-Weld, N. 823786).

References

[1] Miao H, Yusof F, Ab Karim MS, Wu B, Raja S, Ibrahim MZ, et al. Interfacial microstructure, element diffusion, mechanical properties and metallurgical bonding mechanism of 316L-AlSi10Mg multi-material parts fabricated by laser powder bed fusion. J Mater Res Technol 2023;26:8351–65. https://doi.org/10.1016/j.jmrt.2023.09.158.

[2] Baek S, Song J, Lee H, Park S, Song K-H, Lee S, et al. Robust bonding and microstructure behavior of aluminum/high-strength steel lap joints using resistance element welding process for lightweight vehicles: Experimental and numerical investigation. Mater Sci Eng, A 2022;833:142378. https://doi.org/10.1016/j.msea.2021.142378.

[3] Mohd Jamil MZ, Mohd Isa MS, Raja S, bin Muhamad MR, Yusof F, Hasnan HK, et al. Friction stir alloying AZ61 magnesium alloy and mild steel with Zn-CNT additive. Trans Indian Inst Met 2024;77:435–43. https://doi.org/10.1007/s12666-023-03124-8.

[4] Verma R, Sharma L, Chauhan M, Chhibber R, Arora KS. Experimental investigation on adhesive bonding of similar and dissimilar weld joint used for automotive applications. Proc IME E J Process Mech Eng 2022;236:752–61. https://doi.org/10.1177/09544089211063116.

[5] Jana S, Hovanski Y, Grant GJ. Friction stir lap welding of magnesium alloy to steel: a preliminary investigation. Metall Mater Trans 2010;41:3173–82.

[6] bin Ariffin MA, bin Muhamad MR, Raja S, Jamaludin MF, Yusof F, Suga T, et al. Friction stir alloying of AZ61 and mild steel with Cu-CNT additive. J Mater Res Technol 2022;21:2400–15. https://doi.org/10.1016/j.jmrt.2022.10.082.

[7] Sadeghi A, Inoue J, Kyokuta N, Koseki T. In situ deformation analysis of Mg in multilayer Mg-steel structures. Mater Des 2017;119:326–37. https://doi.org/10.1016/j.matdes.2017.01.078.

[8] Nayeb-Hashemi AA, Clark Ljs JB. Binary alloy phase diagrams. Am Soc Microbiol News 1986;2:1772.

[9] bin Muhamad MR, Raja S, Jamaludin MF, Yusof F, Morisada Y, Suga T, et al. Enhancements on dissimilar friction stir welding between AZ31 and SPHC mild steel with Al–Mg as powder additives. J Manuf Sci Eng 2021;143. https://doi.org/10.1115/1.4049745.

[10] Baek S, Ma N, Song J, Kim D-K, Lee S-J, Chen C, et al. Effect of Mg remelting and mechanical hooks of steel on the mechanical and fatigue responses of resistance element welded AZ31/DP780 joints: Experimental, FEM and thermodynamic calculation studies. J Mater Res Technol 2023;22:1210–37. https://doi.org/10.1016/j.jmrt.2022.11.157.

[11] Zhao X, Wang D, Gao J, Jia J, Xu N, Lei Y. The effect of Ni foil on the interface microstructure and mechanical properties of laser lap welded steel/Mg joint. J Mater Res Technol 2022;19:4672–82. https://doi.org/10.1016/j.jmrt.2022.07.030.
[12] Song G, Li T, Chen L. The mechanical properties and interface bonding mechanism of immiscible Mg/steel by laser–tungsten inert gas welding with filler wire. Mater Sci Eng, A 2018;736:306–15. https://doi.org/10.1016/j.msea.2018.08.078.
[13] Raja S, Muhamad MR, Yusof F, Jamaludin MF, Suga T, Liu H, et al. Friction stir alloying of AZ61 and mild steel with Al-CNT additive. Sci Technol Weld Join 2022;27:533–40. https://doi.org/10.1080/13621718.2022.2080449.
[14] Li L, Tan C, Chen Y, Guo W, Song F. Comparative study on microstructure and mechanical properties of laser welded–brazed Mg/mild steel and Mg/stainless steel joints. Mater Des 2013;43:59–65. https://doi.org/10.1016/j.matdes.2012.06.057.
[15] Wang T, Shukla S, Gwalani B, Komarasamy M, Reza-Nieto L, Mishra RS. Effect of reactive alloy elements on friction stir welded butt joints of metallurgically immiscible magnesium alloys and steel. J Manuf Process 2019;39:138–45. https://doi.org/10.1016/j.jmapro.2019.02.009.
[16] Tao T, Liu J, Zhou D, Li C, Li H. Microstructure and mechanical properties of laser welding of AZ31B magnesium alloy and DP590 dual-phase steel with concave groove joint. J Manuf Process 2021;72:227–39. https://doi.org/10.1016/j.jmapro.2021.10.024.
[17] Wu Z, Wan J, Zhang Y, Li C, Liu Y, Yang C. The influence of welding speed on nanosecond laser welding of AZ31B magnesium alloy and 304 stainless steel. Opt Laser Technol 2024;168:109997. https://doi.org/10.1016/j.optlastec.2023.109997.
[18] Li H, Zhou D, Wang X. Oscillating laser welding of AZ31B magnesium alloy to DP590 dual-phase steel. Opt Laser Technol 2023;158:108857. https://doi.org/10.1016/j.optlastec.2022.108857.
[19] Li W, Chang J, Wen B, Cao R. Joining of dissimilar metals between magnesium AZ31B and aluminum A6061-T6 using galvanized steel as a transition joining layer. J Iron Steel Res Int 2022;29:677–86. https://doi.org/10.1007/s42243-021-00589-z.
[20] Zhang D, Zhang X, Wang W, Zheng J, Chu J, Cui L, et al. Weld formation, microstructure and mechanical properties of magnesium alloy and Al-Si-coated steel dissimilar lap joints fabricated by the CMT weld-brazing process. Mater Char 2023;204:113152. https://doi.org/10.1016/j.matchar.2023.113152.
[21] Cao R, Chang JH, Zhu HX, Mao GJ, Xu QW, Shi Y, et al. Investigation of wire selection for CMT plug joining Mg AZ31-to-galvanized steel. J Manuf Process 2018;32:65–76. https://doi.org/10.1016/j.jmapro.2018.01.022.
[22] Liu L, Xiao L, Feng JC, Tian YH, Zhou SQ, Zhou Y. The mechanisms of resistance spot welding of magnesium to steel. Metall Mater Trans 2010;41:2651–61.
[23] Liu L, Zou G, Mori H, Esmaeili S, Zhou YN. Nanostructure of immiscible Mg–Fe dissimilar weld without interfacial intermetallic transition layer. Mater Des 2016;92:445–9. https://doi.org/10.1016/j.matdes.2015.12.072.
[24] Feng Y, Li Y, Luo Z, Ling Z, Wang Z. Resistance spot welding of Mg to electro-galvanized steel with hot-dip galvanized steel interlayer. J Mater Process Technol 2016;236:114–22. https://doi.org/10.1016/j.jmatprotec.2016.05.015.
[25] Ebrahimpour A, Shakoori A, Saeid T. Metallurgical and mechanical study of the effect of FSW parameters on dissimilar joining of St37 and AZ31. Weld World 2023;67:2683–702. https://doi.org/10.1007/s40194-023-01602-7.
[26] Khalaf HI, Al-Sabur R, Derazkola HA. Effect of number of tool shoulders on the quality of steel to magnesium alloy dissimilar friction stir welds. Arch Civ Mech Eng 2023;23:125. https://doi.org/10.1007/s43452-023-00673-z.
[27] Fu X, Chen K, Zhang Q, Chen N, Wang M, Hua X. Interfacial intermetallic compound layer in friction stir welded Mg/Al joints: relationship between thickness and the welding temperature history. J Magnesium Alloys 2023. https://doi.org/10.1016/j.jma.2023.01.010.
[28] Li T, Xie X, Xu J, Li R, Qi K, Zhang X, et al. Research on AZ31 Mg alloy/22MnB5 steel pinless friction stir spot welding process and interfacial temperature field simulation. J Mater Res Technol 2023;26:3710–25. https://doi.org/10.1016/j.jmrt.2023.08.169.
[29] Jun J, Joshi VV, Crawford A, Viswanathan V, Leonard DN, Chen J, et al. Galvanic corrosion of AZ31B joined to dual-phase steel with and without Zn layer by ultrasonic and friction stir welding. J Magnesium Alloys 2023;11:462–79. https://doi.org/10.1016/j.jma.2023.01.016.
[30] Das H, Upadhyay P, Wang T, Gwalani B, Ma X. Interfacial reaction during friction stir assisted scribe welding of immiscible Fe and Mg alloy system. Sci Rep 2021;11:1–8. https://doi.org/10.1038/s41598-021-81266-9.
[31] Fu B, Shen J, Suhuddin UFHR, Pereira AAC, Maawad E, dos Santos JF, et al. Revealing joining mechanism in refill friction stir spot welding of AZ31 magnesium alloy to galvanized DP600 steel. Mater Des 2021;209:109997.
[32] Peng P, Wang K, Wang W, Yang T, Liu Q, Zhang T, et al. Intermetallic compounds: formation mechanism and effects on the mechanical properties of friction stir lap welded dissimilar joints of magnesium and aluminum alloys. Mater Sci Eng, A 2021;802:140554. https://doi.org/10.1016/j.msea.2020.140554.
[33] Li T, Song G, Yu P, Liu L. Interfacial microstructure evolution in fusion welding of immiscible Mg/Fe system. Mater Des 2019;181:107903. https://doi.org/10.1016/j.matdes.2019.107903.
[34] Zhai M, Shi L, Wu C. Elucidating the process mechanism in Mg-to-Al friction stir lap welding enhanced by ultrasonic vibration. J Magnesium Alloys 2023. https://doi.org/10.1016/j.jma.2023.09.032.
[35] Peng H, Chen DL, Bai XF, Wang PQ, Li DY, Jiang XQ. Microstructure and mechanical properties of Mg-to-Al dissimilar welded joints with an Ag interlayer using ultrasonic spot welding. J Magnesium Alloys 2020;8:552–63. https://doi.org/10.1016/j.jma.2020.04.001.
[36] Ahmed MMZ, El-Sayed Seleman MM, Fydrych D, Çam G. Review on friction stir welding of dissimilar magnesium and aluminum alloys: Scientometric analysis and strategies for achieving high-quality joints. J Magnesium Alloys 2023;11:4082–127. https://doi.org/10.1016/j.jma.2023.09.039.
[37] Yamani SM, Raja S, bin Ariffin MA, Mohd Isa MS, Muhamad MR, Jamaludin MF, et al. Effects of Preheating on microstructural and mechanical properties of friction stir welded thin low carbon steel joints. J Eng Mater Technol 2022;145. https://doi.org/10.1115/1.4055909.
[38] Raja S, Shaikh MBN, Majeed M, Varshney A, Samad A. Design, modelling, fabrication, and testing of vertical milling machine fixture for friction stir welding operation. In: Prasad R, Sahu R, Sahoo KL, Jadhav GN, editors. Advancement in materials processing technology. Singapore: Springer Singapore; 2022. p. 95–106. https://doi.org/10.1007/978-981-16-3297-6_9.
[39] Raja S, Muhamad MR, Jamaludin MF, Yusof F. A review on nanomaterials reinforcement in friction stir welding. J Mater Res Technol 2020;9:16459–87. https://doi.org/10.1016/j.jmrt.2020.11.072.
[40] Wu B, Ibrahim MZ, Raja S, Yusof F, binti Abdul Razak B, Bin Muhamad MR, et al. The influence of reinforcement particles friction stir processing on microstructure, mechanical properties, tribological and corrosion behaviors: a review. J Mater Res Technol 2022;20:1940–75. https://doi.org/10.1016/j.jmrt.2022.07.172.
[41] Isa MSM, Moghadasi K, Ariffin MA, Raja S, bin Muhamad MR, Yusof F, et al. Recent research progress in friction stir welding of aluminium and copper dissimilar joint: a review. J Mater Res Technol 2021;15:2735–80. https://doi.org/10.1016/j.jmrt.2021.09.037.
[42] Abdul Khaliq U, Muhamad MR, Yusof F, Ibrahim S, Mohd Isa MS, Chen Z, et al. A review on friction stir butt welding of aluminum with magnesium: a new insight on joining mechanisms by interfacial enhancement. J Mater Res Technol 2023;27:4595–624. https://doi.org/10.1016/j.jmrt.2023.10.158.
[43] Singh VP, Patel SK, Ranjan A, Kuriachen B. Recent research progress in solid state friction-stir welding of aluminium-magnesium alloys: a critical review. J Mater Res Technol 2020;9:6217–56. https://doi.org/10.1016/j.jmrt.2020.01.008.
[44] Singh VP, Patel SK, Kumar N, Kuriachen B. Parametric effect on dissimilar friction stir welded steel-magnesium alloys joints: a review. Sci Technol Weld Join 2019;24:653–84. https://doi.org/10.1080/13621718.2019.1567031.
[45] Wang T, Upadhyay P, Whalen S. A review of technologies for welding magnesium alloys to steels. International Journal of Precision Engineering and Manufacturing-Green Technology 2021;8:1027–42.
[46] Chen YC, Nakata K. Effect of tool geometry on microstructure and mechanical properties of friction stir lap welded magnesium alloy and steel. Mater Des 2009;30:3913–9. https://doi.org/10.1016/j.matdes.2009.03.007.
[47] Kasai H, Morisada Y, Fujii H. Dissimilar FSW of immiscible materials: steel/magnesium. Mater Sci Eng 2015;624:250–5. https://doi.org/10.1016/j.msea.2014.11.060.
[48] Chen J, Shalchi Amirkhiz B, Zhang R. Continuous nanoscale Al2Fe transition layer strengthened magnesium-steel spot joints. Mater Lett 2017;196:242–4. https://doi.org/10.1016/j.matlet.2017.03.020.
[49] Nasiri AM, Weckman DC, Zhou Y. Interfacial microstructure of laser brazed AZ31B magnesium to Snplated steel sheet. Weld J 2015;94:61S–72S.
[50] Xu Y, Ke L, Mao Y, Sun J, Duan Y, Yu L. An innovative joint interface design for reducing intermetallic compounds and improving joint strength of thick plate friction stir welded Al/Mg joints. J Magnesium Alloys 2023;11:3151–60. https://doi.org/10.1016/j.jma.2022.01.007.
[51] Song G, Li T, Yu J, Liu L. A review of bonding immiscible Mg/Steel dissimilar metals. Materials 2018;10:1–25. https://doi.org/10.3390/ma11122515.
[52] Xu RZ, Ni DR, Yang Q, Xiao BL, Liu CZ, Ma ZY. Influencing mechanism of Al-containing Zn coating on interfacial microstructure and mechanical properties of friction stir spot welded Mg–steel joint. Mater Char 2018;140:197–206. https://doi.org/10.1016/j.matchar.2018.04.011.
[53] Ragu Nathan S, Balasubramanian V, Rao AG, Sonar T, Ivanov M, Suganeswaran K. Effect of tool rotational speed on microstructure and mechanical properties of friction stir welded DMR249A high strength low alloy steel butt joints for fabrication of light weight ship building structures. International Journal of Lightweight Materials and Manufacture 2023;6:469–82. https://doi.org/10.1016/j.ijlmm.2023.05.004.
[54] Trzepieciński T, Najm SM. Current trends in metallic materials for body panels and structural members used in the automotive industry. Materials 2024;17. https://doi.org/10.3390/ma17030590.
[55] Taweejun N, Kanchanomai C. Effects of carbon and nitrogen on the microstructure and mechanical properties of carbonitrided low-carbon steel. J Mater Eng Perform 2015;24:4853–62. https://doi.org/10.1007/s11665-015-1757-x.
[56] Khan Furkan, Miura T, Morisada Y, Ushioda K, Fujii H. Dissimilar linear friction welding of 7075-T6 Al and low carbon steel. Preprints of the National Meeting of JWS 2023;2023:108–9. https://doi.org/10.14920/jwstaikai.2023s.0_108.
[57] He G, Peng T, Jiang B, Hu X, Liu Y, Wu C. Recrystallization behavior and texture evolution in low carbon steel during hot deformation in austenite/ferrite region. Steel Res Int 2021;92:2100047. https://doi.org/10.1002/srin.202100047.
[58] R M. P. S. Review on the effect of different processing techniques on the microstructure and mechanical behaviour of AZ31 Magnesium alloy. J Magnesium Alloys 2021;9:1692–714. https://doi.org/10.1016/j.jma.2021.03.019.
[59] Liu Y, Yu D, Zhang Y, Zhou J, Sun D, Li H. Research advances on weldability of Mg alloy and other metals worldwide in recent 20 years. J Mater Res Technol 2023;25:3458–81. https://doi.org/10.1016/j.jmrt.2023.06.184.
[60] Prangnell PB, Heason CP. Grain structure formation during friction stir welding observed by the 'stop action technique. Acta Mater 2005;53:3179–92. https://doi.org/10.1016/j.actamat.2005.03.044.

[61] Beygi R, Galvão I, Akhavan-Safar A, Pouraliakbar H, Fallah V, da Silva LFM. Effect of alloying elements on intermetallic formation during friction stir welding of dissimilar metals: a critical review on aluminum/steel. Metals 2023;13. https://doi.org/10.3390/met13040768.

[62] Naoi D, Kajihara M. Growth behavior of Fe2Al5 during reactive diffusion between Fe and Al at solid-state temperatures. Mater Sci Eng, A 2007;459:375–82. https://doi.org/10.1016/j.msea.2007.01.099.

[63] Bouayad A, Gerometta C, Belkebir A, Ambari A. Kinetic interactions between solid iron and molten aluminium. Mater Sci Eng, A 2003;363:53–61. https://doi.org/10.1016/S0921-5093(03)00469-6.

[64] Xu L, Robson JD, Wang L, Prangnell PB. The influence of grain structure on intermetallic compound layer growth rates in Fe-Al dissimilar welds. Metall Mater Trans 2018;49:515–26. https://doi.org/10.1007/s11661-017-4352-y.

[65] Zhang Z, Wang X, Wang P, Zhao G. Friction stir keyholeless spot welding of AZ31 Mg alloy-mild steel. Trans Nonferrous Metals Soc China 2014;24:1709–16. https://doi.org/10.1016/S1003-6326(14)63244-1.

[66] Liu L, Xiao L, Feng J, Li L, Esmaeili S, Zhou Y. Bonding of immiscible Mg and Fe via a nanoscale Fe2Al5 transition layer. Scripta Mater 2011;65:982–5. https://doi.org/10.1016/j.scriptamat.2011.08.026.